Nanoscale-nMOSFET Junction Design: Quantum Transport Approach

M. Ali Pourghaderi, Chulwoo Park, Jongchol Kim, Changwook Jeong, Won-Young Chung, Keun-Ho Lee
Semiconductor R&D center
Samsung Electronics
Hwasung-si, Gyeonggi-do, Korea
ali.p@samsung.com

Hong-Hyun Park, Anh-Tuan Pham, Seonghoon Jin, Woosung Choi
Device Lab, AHQ(DS) R&D
Samsung Semiconductor Inc.
San Jose, CA, USA

***Abstract*— Employing quantum transport solver, we have demonstrated the impact of junction proximity and abruptness on device performance. To entail the discrete dopant effect accurately, impurity scattering has been introduced in non-perturbative way. The electrostatic metrics and effective current have been evaluated for practical dimensions and technologically relevant junctions. A simple guideline for junction design has been concluded.**

Keywords—Junction abruptness; discrete dopant; carrier transport

I. INTRODUCTION

Conventionally, logic path finding involves the performance and power evaluation for a given contact-poly-pitch (cpp). The design is expected to optimize the interplay of gate-length, junction profile and channel cross-section in nanoscale dimensions. Dealing with such small devices, we have employed Non-Equilibrium Green's Function (NEGF) machinery to account for quantum transport aspects. This study covers Gaussian junctions in n-type metal-oxide-semiconductor field effect transistors (nMOSFET) with gate-all-around (GAA) architecture, Fig. 1. In the following, the Proximity (PR) indicates the distance between the edge of gate and the base of Gaussian doping profile and junction abruptness, JD, is the characteristic decay length. The peak of source/drain doping is 3×10^{20} cm^{-3}. The channel orientation is <110> and the wide side of the wire is (100) surface.

II. UNIVERSALITY OF SCE AND LEFF ESTIMATION

The proper definition of natural length, λ, and effective gate length, Leff, yields a universal curve for short channel effect (SCE) metrics: drain induced barrier lowering (DIBL) and subthreshold swing (SS) [1, 2]. Fig. 2 and 3 illustrate the ballistic simulation results for various combinations of proximity, channel length (Lg), channel thickness and width. Universal curves have been obtained through polynomial expression of Leff as a function of gate length, PR and JD. Since both λ and Leff are expressed by analytical forms, it is possible to study the relation of different parameters satisfying a given electrostatic constraint. As an example, Fig.4 and 5 show the relation between minimum gate length and channel width as such that resulting devices satisfy DIBL < 30mV/V. In both figures, effective oxide thickness (EOT) is fixed as 0.92nm. The results in Fig. 4 suggest that for a given channel with, 2nm/Dec reduction in JD can save up to 4 nm in gate length. In Fig.5, JD is fixed as 5nm/Dec. To shrink the cpp by 2nm at fixed channel width, we might either thin down the channel by 0.8nm or reduce the PR by 2.5nm. The first option will trigger higher scattering rate of thin channels. Considering the performance, the second option might be more favorable: reducing PR by 2.5nm and increasing Lg by 3nm.

III. PERFORMANCE VS. JUNCTION PROFILE

As a representative of device performance, effective current (Ieff) has been calculated for wide range of junctions and Lg. In the following, channel cross section is fixed as 4.8x24nm and EOT is 0.87nm, unless it is said otherwise. To estimate a realistic performance, electron-phonon interaction (Ph), random dopant and random surface-roughness (SR) have been included in NEGF machinery. The introduced variability is then filtered out by averaging over 30 samples, Fig. 1(c). In this way,

© 2017 The Japan Society of Applied Physics

3D screening of scattering centers has been included accurately.

Fig. 6 shows the impact of dopant concentration on channel mobility. To account for 3D screening of impurity scattering, six different Lg have been simulated for each channel concentration (NCh). Then, the resulting apparent mobilities have been decomposed to the ballistic and effective mobility components. Compared to undoped devices (Ph+SR), effective mobility at strong inversion starts to degrade around $3x10^{18}$ cm^{-3} (~10% loss) and continues to decrease further for higher NCh: 20% loss at $1x10^{19}$ cm^{-3}. The mobility degradation is more pronounced, almost 2x, around the threshold voltage.

Fig. 7 shows the typical behavior of Ieff as a function of PR. The optimum performance (symbols) will be obtained somewhere between deep-underlap and deep-overlap design. Compare to analytical junction results, the mere impurity scattering hampers the performance by less than 9%. In case of slow junctions, JD=6nm/Dec, big portion of this degradation comes from dopant in channel area (w.r.t dashed line), while this portion is negligible for the sharpest junction. This conclusion is consistent with result in Fig. 6 if the average number of dopant in short Lg is taken into account.

The very *"bell"* shape of performance curve can be explained by combination of electrostatic and carrier back scattering, Fig. 8. To estimate the performance loss due to electrostatic, we have applied identical overdrive voltages to different PR designs. The full-lines in Fig. 8 represent the performance loss w.r.t fixed-overdrive calculations. As expected, electrostatic loss is minimal for longer Leff, large PR, and rapidly increases for deep-overlap designs, where shorter Leff yields poor SS, like Fig. 2. On the other hand, very large PR comes with poor carrier injection. Clearly, if a certain level of overlap is not secured, carriers will experience huge back scattering even before they enter the channel area. As the results, moving away from deep-underlap, the performance will rapidly increase due to initial injection boost. Once the optimum carrier injection is obtained, extra overlap will put more dopant in channel and impurity scatting will hamper the carrier transmission, as depicted by dashed line in Fig. 8.

Fig. 9 shows the overlap and underlap design performance for different Lg. The peculiar feature of these curves is that the peak value is almost insensitive to choice of JD. Fig .10 shows the effective electric field for optimum combination of JD and PR. For sharper junction, the peak of electric field is slightly higher and it is more confined in channel region. Contrary to slower junctions, where the electric field is more expanded in extension region and the peak is slightly lower. In overall, the driving force by electric field seems similar for optimum combinations. We may conclude that different JD will produce very similar performance peak if Leff is designed properly. Fig. 11 demonstrates the saturation velocity and current for different gate lengths at optimum combination of PR and JD. The extraction is performed based on virtual source model [3]. The identical slope of lines in Fig. 11(b) indicates that the transmission rate can be similar for different scatterer distributions, like Fig. 1(d). This is in fact quite plausible due to nonlocality of impurity scattering.

Finally, Fig .12 shows the impact of misalignment in junction position. The variation of effective current is asymmetric. This is due to inefficient carrier injection triggered by large underlap.

IV. CONCLUSION

Employing quantum transport tool (NEGF), we have studied Gaussian junctions in n-MOSFET nanoscale devices. This study concludes that junction parameters control the effective current mainly through the swing and Leff. If the carrier injection is secured by enough overlap, the role of junction profile can be largely explained by Leff and corresponding swing. The main gain of sharper junctions is to offer the optimum Ieff at smaller PR and consequently shorter cpp. Therefore, to keep the performance in ultra-scaled cpp sharp junctions are essential.

REFERENCES

[1] S. Bangsaruntip, *et all.* "Universality of short-channel effects in undoped-body silicon nanowire MOSFETs",*IEEE Trans Electron Devices*, vol. 31, NO.9, SEPTEMBER. 2010.

[2] K. J. Kuhn. "Considerations for ultimate CMOS scaling ", *IEEE Trans Electron Devices*, vol.59, NO.7, JULY. 2012.

[3] S. Rakheja, *et all*, "A physics-based compact model for FETs from diffusive to ballistic carrier transport regimes" .IEDM, Dec. 2014, pp. 35.1.1-35.1.4.

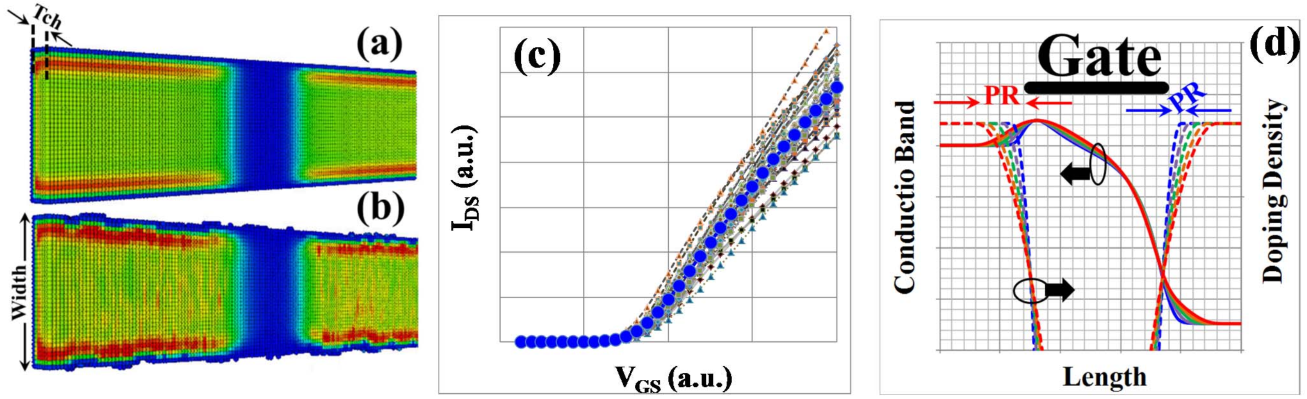

Fig. 1. Electron density profile without (a) and with (b) random fluctuation for typical GAA device. Width of device refers to the wide side of the wire. The resulting current fluctuation is filtered by simple averaging (c). Definition of PR has been demonstrated in (d).

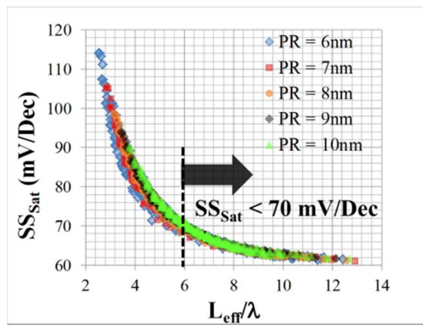

Fig. 2. Universality of subthreshold swing for variant combinations of proximity, gate length and channel cross section. Junction abruptness has been fixed as 5nm/Dec and EOT is 0.92nm.

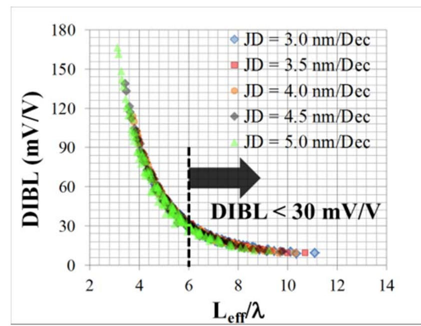

Fig. 3. Universality of DIBL for variant combinations of junction abruptness, gate length and channel cross section. Proximity has been fixed as 7.5nm and EOT is 0.92nm.

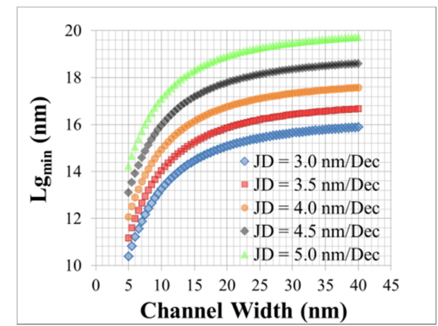

Fig. 4. The minimum gate length consistent with nominal electrostatic criteria (DIBL<30 mV/V). Channel thickness and proximity length have been fixed as 5.2 and 7.5nm, accordingly. Lg lines are almost parallel to each other. For both wide and narrow devices, sharper junctions offer identical Lg saving.

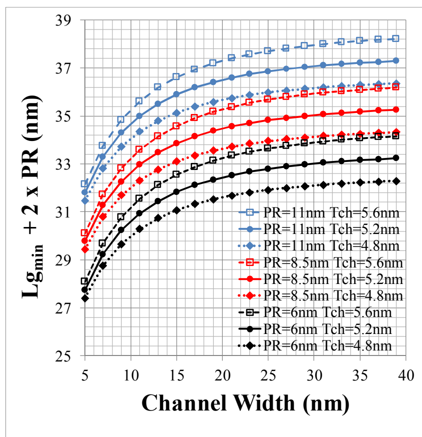

Fig. 5. Reduced cpp (excluding the contact area) consistent with nominal electrostatic criteria (DIBL<30 mV/V). Junction abruptness has been fixed as 5 nm/Dec.

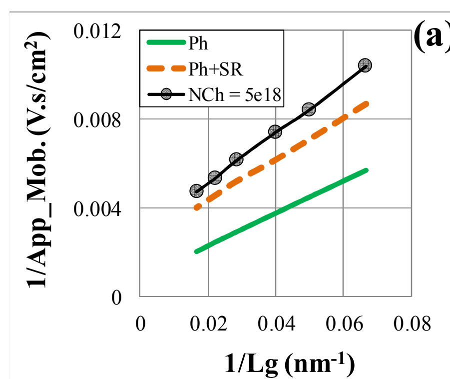

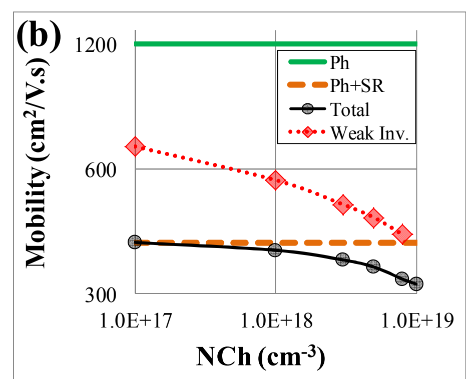

Fig. 6. Reciprocal of apparent mobility for six different Lg: 15, 20, 25, 35, 45 and 60 nm (a). The y-axes intersect has been interpreted as the reciprocal of effective mobility. Channel doping is uniform and both PR and JD are set to zero. The result is obtained for 10mV drain-source voltage and 0.5 V overdrive. The resulting effective mobilities are shown in (b), where total mobility refers to Ph+SR+impurity-scattering. The same calculation has been done for 0.05V overdrive indicated by weak inversion.

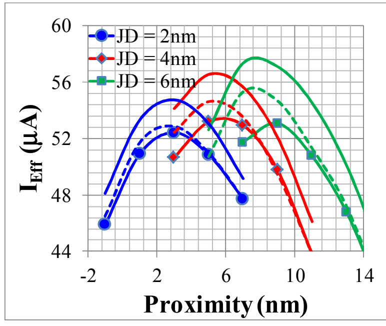

Fig. 7. Decomposition of impurity scattering effect for Lg=18nm. Full line refers to simulations without impurity scattering. Dashed lines refer to no impurity scattering in channel region. Marks refer to impurity scattering everywhere.

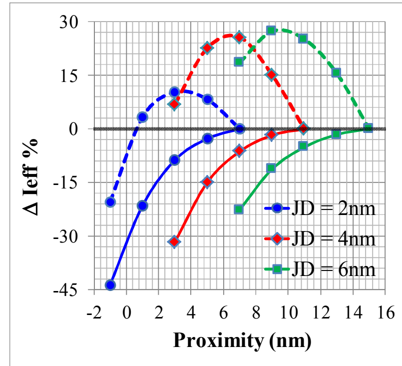

Fig. 8. Decomposition of ΔIeff with reference to deep-underlap designs. Full lines represent the deviation from fixed overdrive simulation, where the dashed line shows the performance improvement due to higher carrier transmission rate.

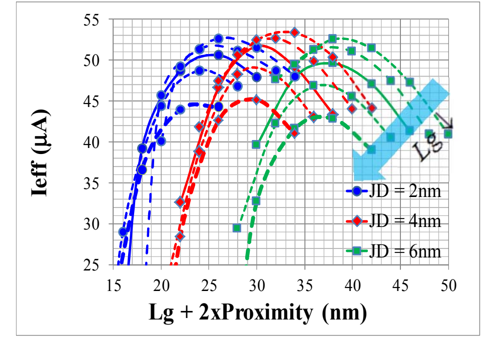

Fig. 9. Ieff for different junctions and cpp lengths. Different colors and line styles correspond to variation of JD and Lg, respectively. Lg range covers 12, 14, 16, 18 and 20 nm, with down scaling in arrow direction. For the fixed JD and cpp, longer Lg gives the better swing and higher Ieff (Lg<20nm).

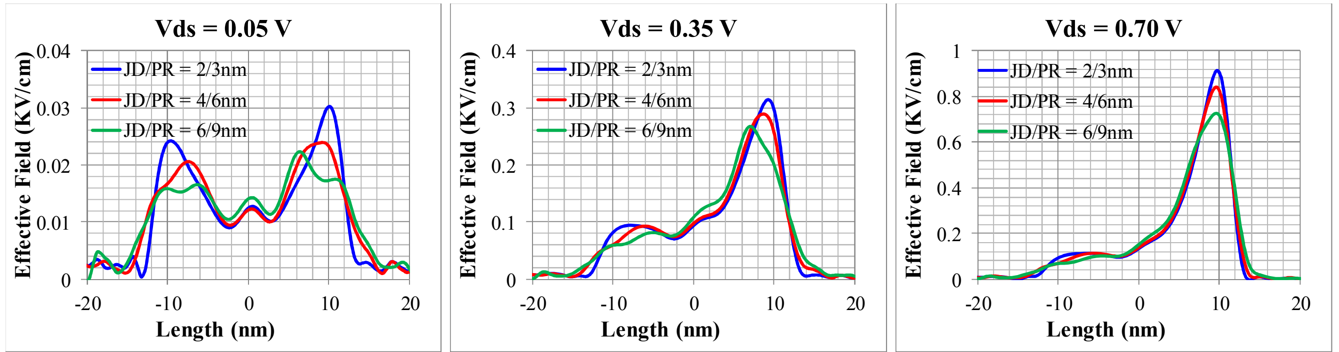

Fig. 10. Effective electric field for Lg=22nm and 0.5V overdrive. To filter the impact of built-in potential, average conduction band at Vds =0 V has been subtracted and then spatial gradient has been carried out. The noise in the data is due to random position of discrete dopants. Sharper junctions give more confined profile and consequently higher peak values.

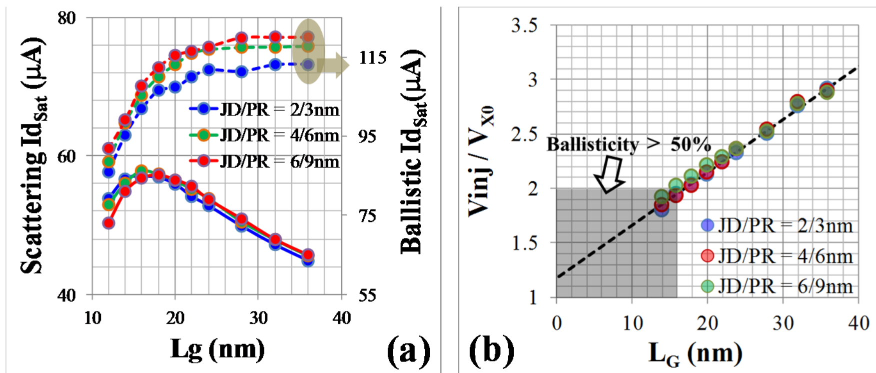

Fig. 11. Saturation current and reciprocal of saturation velocity, V_{x0}, for optimum combination of proximity and junction abruptness. Vinj is the ballistic injection velocity calculated for the same structure. Gate overdrive is fixed as 0.5V. Phonon and surface roughness scattering rate are almost twice compared to Fig. 7-9.

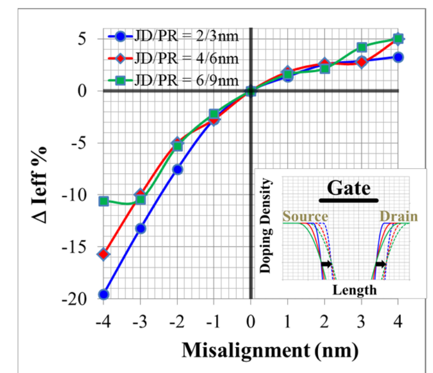

Fig. 12. Variation of Ieff due to junction misalignment. The positive values are corresponding to more overlap on source side (inset).